Nucleic Acids Research Advance Access published August 29, 2016

Nucleic Acids Research, 2016 **1**
doi: 10.1093/nar/gkw752

Intersection of calorie restriction and magnesium in the suppression of genome-destabilizing RNA–DNA hybrids

Karan J. Abraham[1,†], Janet N.Y. Chan[1,†], Jayesh S. Salvi[1,†], Brandon Ho[2], Amanda Hall[1], Elva Vidya[1], Ru Guo[1], Samuel A. Killackey[1], Nancy Liu[1], Jeffrey E. Lee[1,3], Grant W. Brown[2] and Karim Mekhail[1,3,*]

[1]Department of Laboratory Medicine and Pathobiology, Faculty of Medicine, University of Toronto, 1 King's College Circle, Toronto, ON M5S 1A8, Canada, [2]Department of Biochemistry and Donnelly Centre, University of Toronto, 160 College Street, Toronto, ON M5S 3E1, Canada and [3]Canada Research Chairs Program, Faculty of Medicine, University of Toronto, 1 King's College Circle, Toronto, ON M5S 1A8, Canada

Received June 22, 2016; Revised August 18, 2016; Accepted August 20, 2016

ABSTRACT

Dietary calorie restriction is a broadly acting intervention that extends the lifespan of various organisms from yeast to mammals. On another front, magnesium (Mg^{2+}) is an essential biological metal critical to fundamental cellular processes and is commonly used as both a dietary supplement and treatment for some clinical conditions. If connections exist between calorie restriction and Mg^{2+} is unknown. Here, we show that Mg^{2+}, acting alone or in response to dietary calorie restriction, allows eukaryotic cells to combat genome-destabilizing and lifespan-shortening accumulations of RNA–DNA hybrids, or R-loops. In an R-loop accumulation model of Pbp1-deficient *Saccharomyces cerevisiae*, magnesium ions guided by cell membrane Mg^{2+} transporters Alr1/2 act via Mg^{2+}-sensitive R-loop suppressors Rnh1/201 and Pif1 to restore R-loop suppression, ribosomal DNA stability and cellular lifespan. Similarly, human cells deficient in ATXN2, the human ortholog of Pbp1, exhibit nuclear R-loop accumulations repressible by Mg^{2+} in a process that is dependent on the TRPM7 Mg^{2+} transporter and the RNaseH1 R-loop suppressor. Thus, we identify Mg^{2+} as a biochemical signal of beneficial calorie restriction, reveal an R-loop suppressing function for human ATXN2 and propose that practical magnesium supplementation regimens can be used to combat R-loop accumulation linked to the dysfunction of disease-linked human genes.

INTRODUCTION

The longevity of various organisms is intimately linked to the lifespan of their cells (1,2). Research in the past few decades has revealed that cellular and organismal lifespan can be genetically or pharmacologically modulated opening the door for a line of thought that views aging as a malleable biological process that can be significantly, and fortunately, stalled (2,3).

Calorie restriction (CR), or a decrease in dietary glucose intake, is the most effective strategy to extend the lifespan of healthy or diseased cells (2,3). Major interconnected processes mediating beneficial effects of CR include the constriction of glycolysis, activation of the nicotinamide adenine dinucleotide (NAD^+)-dependent histone deacetylase Sir2 (founding member of the conserved family of sirtuin longevity proteins), inhibition of TOR (target of rapamycin) and stabilization of the highly repetitive and thus genome destabilization prone ribosomal RNA gene repeats (*rDNA*) (4–11).

Living organisms typically harbor hundreds to thousands of *rDNA* units per cell necessary to meet its protein translation needs (10). We recently reported that, in the budding yeast *Saccharomyces cerevisiae*, CR can promote *rDNA* stability by abolishing deleterious accumulations of nucleic acid structures called R-loops (12,13). These are formed when nascent RNA competes with the DNA double helix hybridizing with one DNA strand while displacing the other. R-loops can be particularly stable if the displaced single-stranded DNA harbors so called

*To whom correspondence should be addressed. Tel: +1 416 946 8132; Fax: +1 416 978 5959; Email: karim.mekhail@utoronto.ca
†These authors contributed equally to this work as the first authors.
Present address: Jayesh S. Salvi, The Glenn Laboratories for the Biology of Aging and Department of Neurology and Neurological Sciences, Stanford University School of Medicine, Stanford, CA 94305, USA.

G-quadruplex-DNA (G4DNA) sequences that lock this displaced DNA strand into a looping structure (12,14). Although many biological processes including eukaryotic gene expression can be beneficially controlled by R-loops, their aberrant accumulation compromises genome stability in different organisms from yeast to human. In fact, genes mutated in various human diseases including cancer and neurodegeneration have recently emerged as suppressors of R-loop accumulation (13,15). This highlights the importance of identifying broadly effective and practical strategies to combat deleterious R-loop buildup.

R-loops stably accumulate at G4DNA-containing sites within the intergenic regions of *rDNA* in yeast cells lacking the conserved RNA-binding factor Pbp1, which is orthologous to the human ATXN2 gene product mutated in some neurodegenerative diseases (12,16,17). R-loop buildup interferes with *rDNA* replication triggering cellular lifespan-shortening aberrant recombination within the repeats (12,18). Subjecting Pbp1 knockout (*pbp1Δ*) cells to a CR regimen that entails decreasing glucose concentration from 2% to 0.05% abolishes R-loop buildup restoring *rDNA* stability and cellular lifespan via a process that somehow requires two highly conserved R-loop suppressors, Pif1 and Rnh1/201 (RNaseH enzymes Rnh1 and Rnh201) (12). Pif1 is a helicase that suppresses R-loops by resolving G4DNA and RNA–DNA hybrids (19,20). RNaseH enzymes degrade the RNA component of hybrids and have been recently shown to counter deleterious R-loop accumulations *in vivo* (21,22).

Importantly, mammalian CR responses depend on highly specific diets that generally include a 20–40% decrease in daily caloric intake, conditions that are too complicated and most likely too severe for individuals already suffering from disease (2). Therefore, we aimed to gain insight into yeast responses to CR in an effort to identify more direct and practical interventions that can potentially counter R-loop accumulation in both yeast and human cells, which are separated by over a billion years of evolution.

By first investigating the potential impact of CR on common effectors of yeast Pif1 and Rnh1/201 enzymes, we uncovered a CR-induced Mg^{2+}-driven cascade that culminates in R-loop repression. CR increases intracellular Mg^{2+} by boosting the expression of major Mg^{2+} transporters. Disrupting these transporters or decreasing environmental Mg^{2+} levels compromises CR-dependent repression of R-loop buildup in *pbp1Δ* cells. Supplementing cells directly with Mg^{2+} without CR targets R-loop suppressors, counters R-loop accumulation, restores rDNA stability and increases lifespan in Pbp1-deficient cells. In an effort to assess the evolutionary conservation of processes uncovered in yeast, we identified human ATXN2 as an R-loop suppressor and found that Mg^{2+} supplementation counters R-loop accumulation in ATXN2-deficient human cells by a process that requires analogous Mg^{2+} transporters and R-loop suppressors. Taken together, our work identifies Mg^{2+} as a biochemical signal of beneficial calorie restriction and shows that magnesium supplementation can be used to combat R-loop accumulation pertinent to various human diseases.

MATERIALS AND METHODS

Yeast strains and materials

Endogenous genes were deleted as described (23). Yeast strains and primers used are listed (Supplementary Tables S3 and S4). R-loop detection via direct pull downs employed the anti-RNA–DNA antibody from Kerafast (cat# ENH001), which exhibited lower enrichments but higher specificity compared to antibodies that we used previously in chromatin immunoprecipitation (ChIP) (12). Anti-RNAPII, anti-diAcH3K9/14, anti-TAP and anti-β-Actin antibodies were purchased from BioLegend (665004), Millipore (06-599), Sigma (P1291-500UL) and Thermo Scientific (MA1-744), respectively. Anti-GFP was a kind gift from D. Moazed (Harvard University). The Stm1 YEplac181 plasmid or empty vector control were kind gifts from F.B. Johnson (University of Pennsylvania) (24).

Yeast caloric restriction and environmental Mg^{2+} modulation

Media containing 0.05% glucose, instead of the standard 2% glucose, was used in YEP media for CR treatment (12,25). For yeast Mg^{2+} supplementation, 100 mM $MgCl_2$ or $CaCl_2$ was used unless otherwise indicated. For environmental Mg^{2+} depletion experiments, synthetic complete media was made using Yeast Nitrogen Base lacking magnesium (Formedium, CYN2801) before adding $MgCl_2$ to a normal level of 10 mM or depleted level of 1 mM. Media was always replenished after overnight growth to ensure that cells were not glucose starved.

Magnesium concentration measurements

Exponentially growing yeast cells were harvested (5.0×10^7) in 0.75 ml of growth media and 0.25 ml of growth media containing 1 mM MagnesiumGreen (Life Technologies: M-3735) was added. Cell-MagnesiumGreen mixture was allowed to incubate for 45 min at 30°C with rotation. Cells were washed three times in growth media and allowed to incubate for an additional 30 min at 30°C with rotation. A total of 0.25 ml of cells was transferred to clear flat-bottomed 96-well plate. Absorbance was measured with a Perkin Elmer Victor3 plate reader. Relative magnesium concentration in arbitrary absorbance units was calculated using Beer's law and the following formula: $[Cells_{Mg2+}] / [Media_{Mg2+}] = Absorbance_{Cells} / Absorbance_{Media}$, where 'Media' represents the growth media/magnesium-green mixture.

Yeast ChIP

ChIP analysis was performed as described with minor modifications (12,23,26). For standard ChIP assays, overnight yeast cultures (25 ml) were diluted to 50 ml with fresh media and were grown to an OD_{600} of 1.8 and cross-linked with 1% formaldehyde at room temperature (RT) for 30 min. The reaction was quenched with glycine at a final concentration of 125 mM for 5 min at RT. Cells were washed with cold TBS (20 mM Tris-HCl pH 7.6 and 150 mM NaCl). Cell pellets were resuspended in 400 μl of lysis buffer [50 mM HEPES-KOH pH 7.5, 500 mM NaCl, 1 mM EDTA,

1% Triton X-100, 0.1% sodium deoxycholate, 0.1% SDS, 1 mM PMSF, complete protease inhibitor (Roche)]. Cells were bead-beated with an equal volume of glass beads twice for 30 s with intermittent 2 min incubation on ice. Lysates were sonicated 3 times for 20 s at 40% amplitude with intermittent incubations on ice. Two consecutive rounds of centrifugation at 16 000 r.c.f. for 5 and 15 min clarified lysates. For non-TAP IP, 150 μl of lysate was incubated at 4°C for 2 h with 2.0 μg of antibody and further incubated with 30 μl of 50% slurry of pre-washed Protein A-Sepharose beads at 4°C for 1 h. For anti-TAP IP, 150 μl of lysate was incubated with 30 μl of 50% slurry of pre-washed IgG Fast-Flow beads at 4°C for 2 h. Beads were washed 3 times with lysis buffer, once with LiCl buffer (10 mM Tris-HCl pH 8.0, 250 mM LiCl, 0.5% NP-40, 0.5% sodium deoxycholate, 1 mM EDTA) and once with TE (10 mM Tris-HCl pH 8.0, 1 mM EDTA), before elution with 50 mM Tris-HCl pH 8.0, 10 mM EDTA and 1% SDS. The eluate was incubated at 65°C overnight. RNaseA was added at a final concentration of 0.2 μg/μl and incubated at 37°C for 30 min, followed by proteinase K (to 0.2 μg/μl) and glycogen (to 0.03 μg/μl) treatment for 2 h at 37°C. Dilutions for IP and input DNA were 1:2 and 1:1000, respectively. Primers are listed in Supplementary Table S4. For qPCR analyses, IP signals were divided by Input signals and normalized to *CUP1* controls using the following calculations: $[100 \times 2 \wedge (\text{Adjusted Input}_{\text{Gene}} - \text{Adjusted IP}_{\text{Gene}})] / [100 \times 2 \wedge (\text{Adjusted Input}_{\text{CUP1}} - \text{Adjusted IP}_{\text{CUP1}})]$, where $\text{Adjusted Input} = \text{CT}_{\text{Input}} - \log_2 1000$ and $\text{Adjusted IP} = \text{CT}_{\text{IP}} - \log_2 2$. Standard deviations are shown. For EtBr-stained gel-based visualizations, relative fold enrichments were obtained according to the following calculations: $[rDNA_{\text{IP}} / CUP1_{\text{IP}}] / [rDNA_{\text{Input}} / CUP1_{\text{Input}}]$.

Quantitative PCR (qPCR)

Quantitative real-time PCR was performed using the Bio-Rad CFX Connect Real-Time system. Ten microliters qPCR reactions contained 2X SsoAdvanced SYBR Green Supermix (Bio-Rad) or SensiFAST SYBR No-ROX qPCR (FroggaBio, BIO-98020), 200 nM for each of the forward and reverse primers and 1 μl of 10 ng/μl of genomic DNA, diluted Input or IP ChIP DNA. PCR parameters were 1 cycle of 95°C for 35 s, 60°C for 30 s, followed by 39 time of 95°C for 5 s, 60°C for 30 s and the final melt curve at 65°C to 95°C in 0.5°C increment at 5 s/step.

RNA extraction

Total RNA was prepared from logarithmically growing cells using hot phenol. Cells were resuspended in 400 μl of AE buffer [50 mM NaOAc (pH 5.3), 10 mM EDTA, in 0.1% DEPC ddH_2O] and 40 μl of 10% SDS was added. RNA was extracted using 440 μl of acidic phenol (pH 4.5), vortexed and incubated at 65°C for 4 min. The samples were rapidly chilled on dry ice/EtOH bath until crystals appeared before centrifugation for 5 min at 16 000 r.c.f. at RT. The upper phase was transferred to a fresh tube, and 1 volume of phenol:chloroform 5:1 was added. The sample was then centrifuged at 16 000 rcf for 5 min at 4°C. The upper phase was transferred to a new tube before RNA precipitation. One-tenth volume of 3M NaOAc (pH 5.3) and 2.5 volumes of cold 100% EtOH were added, mixed and centrifuged at 16 000 r.c.f. for 5 min at 4°C. Upon removal of the supernatant, the RNA pellet was washed with 2.5 volumes of 80% EtOH. A total of 0.1% DEPC ddH_2O was used to resuspend the pellet. A260:A280 and A260:A230 ratios from Nanodrop confirmed RNA quality. Samples were stored in −20°C until further use.

DNase-I treatment and reverse transcription (RT)

One microgram of total RNA was treated with 1 unit of DNase-I (Invitrogen) to further remove genomic DNA contaminations. Twenty microliters RT reactions were carried out using 10 mM dNTPs, 50 μM random nonamers (Sigma), 500 ng total RNA, 5X First-Strand Buffer (Invitrogen), 100 mM DTT, 40 U/μl RNaseOUT (Invitrogen) and 200 U/μl M-MLV reverse transcriptase (Invitrogen) at 23°C for 10 min, 37°C for 60 min and 70°C for 15 min. Twenty microliters minus-RT reaction without M-MLV reverse transcriptase was also set up in parallel. The RT reaction was diluted 1:4 and 4 μl were used in qPCR amplification. Linearity tests were performed and primers are listed in Supplementary Table S4.

USCE

Assays were performed as described by counting half-sectored colonies grown on media containing low adenine concentration (8,23). Cells were grown to $OD_{600} = 0.4–0.8$, sonicated briefly and spread (about 400 cells per plate) on thick plates (5 mg/l adenine). Incubation was at 30°C for 3 days, 4°C for 3 days, then RT for 1 day. Rates were obtained by dividing the number of half-sectored colonies by the total number of colonies excluding completely red colonies. For Mg^{2+} supplementation unequal sister chromatid exchange (USCE) experiments, cells were grown overnight under 100 mM Mg^{2+} conditions, re-diluted, further grown to $OD_{600} = 0.4–0.8$ and then plated on low adenine concentration media.

Yeast replicative lifespan analyses

Replicative lifespan of yeast strains was determined by micromanipulation monitoring the number of times that an initially new mother cell buds (8). Strains being compared to each other were analyzed in parallel but may be shown on separate plots for clarity as indicated in Supplementary Table S2. The Wilcoxon rank-sum statistical test was conducted.

Yeast cell culture for DNA Combing

Asynchronous cultures were grown in YPAD liquid medium in a water bath shaker at 30°C to early logarithmic phase (OD_{600} ~0.20–0.30). Cells were arrested in G_1 phase with 0.83 μl of 5 mg/ml alpha-factor per ml of culture volume for 75 min. An additional 0.33 μl/ml of 5 mg/ml alpha-factor was added for another 45 min. Cells were labeled with BrdU by incubating cells with 400 μg/ml for 30 min and then releasing into S-phase with 100 μg/ml pronase for 20 min before harvesting.

Agarose plug preparation for DNA combing

Cells were harvested by centrifuging 1.2×10^8 cells in pre-chilled tubes at 3000 r.p.m. for 2 min at 4°C. Cells were washed in ice cold TE_{50} buffer (10 mM Tris-Cl, pH 7.0, 50 mM EDTA) and resuspended in 160 μl SCE buffer (1 M sorbitol, 100 mM sodium citrate, 10 mM EDTA pH 8.0, 0.125% β-mercaptoethanol, 10 U/ml zymolase). Cells were gently mixed with 200 μl of pre-melted 1% low melting point agarose, and 110 μl of the resulting mixture was transferred into a plug mold (BioRad 170–3713) for a total of 3 plugs per sample. Once solidified, plugs were incubated in 0.5 ml SCE buffer per plug at 37°C two days, switching with fresh SCE buffer each day. Plugs were rinsed 3 × 1 ml TE_{50} buffer, and incubated with proteinase K solution (1 mg/ml proteinase K, 1% w/v sarkosyl, 10 mM Tris-Cl pH 7.5, 50 mM EDTA, heated to 50°C for 30 min before use) for 3 days, switching with fresh proteinase K solution each day. Plugs were removed from proteinase K solution and washed 5 times 10 min in TE_{50} at room temperature. Plugs were stored in 1 ml TE_{50} at 4°C protected from light.

Plug melting, molecular combing and immunodetection

Experiments were generally done as described (27). One plug was incubated in 150 μl of YOYO-1 solution (1 μl of YOYO-1 in 150 μl TE_{50}) at room temperature for 30 min. Plugs were washed 3 times for 5 min with 10 ml TE_{50} then incubated in MES buffer (7:3 v/v MES hydrate: MES sodium salt, 50 mM, pH 5.7) for 5 min. MES buffer was removed and replaced with 2 ml fresh MES buffer, and incubated at 72°C for 10–15 min. DNA was combed onto a silanized coverslip at a constant speed of 710 μm/s and hybridized at 60°C for 90 min. Upon mounting onto glass slides, coverslips were dehydrated sequentially in 70%, 90% and anhydrous ethanol for 5 min each, and DNA was denatured in 1 M NaOH for 25 min. Coverslips were blocked in 21 μl blocking buffer (10% w/v albumin in PBS-T, 0.05% Tween-20, 2 mM KH_2PO_4, 2.7 mM KCl, 137 mM NaCl, pH 7.4) for 30 min, and stained with anti-BrdU solution (BrdU antibody Becton Dickson 347580 1:10 dilution in blocking buffer), anti-DNA solution (Millipore MAB3034 1:50 dilution in blocking buffer), and anti-secondary solution (Alexa Fluor 546 anti-mouse IgG1, Molecular Probes A21123, 1:50 dilution, Alexa fluor 648 anti-mouse IgG2, Molecular Probes A21241, 1:50 dilution in blocking buffer) for 1 h at 37°C in a humidity chamber, washing with PBS-T for 5 min three times between each staining. ProLong Gold was added to the cover slip and then imaged.

DNA electrophoresis

2D gel analysis was performed as described (12). Briefly, Bgl-II-digested gel plugs were run on a 0.4% agarose gel for 14 h at 1.32 V/cm. Lanes were excised, rotated 90 degrees and run on 1.2% agarose gel at 6.0 V/cm for 6 h. Replication arcs were analyzed following standard Southern blotting using an alpha-P32-labeled rDNA probe.

Human cells, materials and Mg^{2+} supplementation

HeLa parental and stable shRNA-expressing cell lines were grown in Dulbecco's Modified Eagle's Medium with 10% fetal bovine serum (FBS). Stable HeLa cell lines were generated using shAXTN2 and shCtl plasmids (Oligoengine). All cell lines were cultured in a 37°C incubator with 5% CO_2 in a humidified atmosphere.

The following siRNAs were used in transient knockdown experiments involving human cell lines: siCtl. (Silencer Select), siRNaseH1 (SilencerSelect; Cat #4390826), siTRPM7 (Silencer Select #s29516), siPIF1 (ON-TARGETplus SMARTpool; cat# L-014564-01), siMAGT1 (Silencer Select #s224928) and siBRCA2 (Dharmacon; ON-Targetplus SMARTpool siRNAs L-003462-00-0005). Lipofectamine RNAiMAX (Life technologies) was used for all siRNA transfections and polyethylenimine was used for all RNaseH1 overexpression experiments in human cells.

The following antibodies were used for human cell immunofluorescence: rabbit anti-ATXN2 (Sigma cat# HPA021146), rabbit anti-RNaseH1 (Proteintech cat# 15606-1-AP), mouse anti-B23 (Sigma cat# B0556), mouse anti-UBF1 (Santa Cruz cat# sc-13125) and anti-RNA–DNA S9.6 (Kerafast). For immunoblotting, rabbit anti-ATXN2 (Novus cat# NBP-90063) was used at 1:1000.

For human supplementation experiments, media containing 10 mM $MgCl_2$ was prepared fresh prior to every experiment and regular media was replaced with Mg^{2+}-supplemented media or vehicle only media 24 h prior to experiments such as immunofluorescence or Western blotting.

Human knockdowns and plasmid transfections

For siRNA-dependent knockdown of TRPM7 and MAGT1, shATXN2 cells were seeded in 6-well plates and transfected with a final in-media concentration of 5 nM of siCtl, siTRPM7 or siMAGT1. Forty eight hours after post-transfection, cells were harvested and 1×10^5 cells were re-seeded onto poly-L-lysine (PLL) coated coverslips in either vehicle or 10 mM Mg^{2+}-supplemented medium. For each treatment, at least three replicates were used for immunofluorescence and imaging analysis. Twenty four hours later, cells were fixed and subjected to S9.6 immunofluorescence as described further below.

For RNaseH overexpression analysis, HeLa stable cell lines were seeded in 6-well plates and transfected 24 h later with 0.9 μg pcDNA3-Empty or pcDNA3-RNaseH1. Forty eight hours post-transfection, cells were harvested and re-seeded onto PLL-coated coverslips, which were processed for IF 24 h later using anti-RNA–DNA S9.6 and anti-RNaseH1 to quantify RNA–DNA hybrids and confirm RNaseH1 overexpression, respectively.

For BRCA2 knockdown, 2×10^5 HeLa parental cells were plated in 6-well plates and transfected the next day with a final in-media concentration of 5 nM siControl or siBRCA2 (Dharmacon). Twenty four hours post transfection, cells were harvested and 1×10^5 cells re-seeded onto poly-L-lysine coated coverslips in either vehicle or 10 mM Mg^{2+}-supplemented medium. For each treatment, at least three replicates were processed for subsequent IF and imaging analysis. Twenty four hours later, cells were fixed and subjected to S9.6 immunofluorescence as described below.

Human cell immunofluorescence

Cells were fixed using 1% formaldehyde for 15 min, washed 3 times with 1X PBS, permeabilized with 0.3% TritonX-100 and then washed again three times with phosphate buffered saline (PBS). Coverslips were blocked using 5% bovine serum albumin for 1 h at RT and transferred to humidified chambers for antibody incubations. Coverslips were incubated with 60 μl of primary antibody for 1 h at RT with concentrations as follows: 1:250 anti-ATXN2 (Sigma HPA021146), 1:250 anti-RNaseH1 (Proteintech, 15606-1-AP), 1:200 anti-B23 (Sigma, B0556) and 1:250 anti-UBF1 (Santa Cruz sc-13125). For all S9.6 R-loop immunofluorescence experiments, 1:500 of the antibody was used. After washing with PBS, cells were incubated with secondary antibody for 1 h in a dark chamber. Following further washing and DAPI staining, coverslips were mounted onto microscope slides using DAKO fluorescent mounting medium and then sealed with nail polish.

Microscopy

We employed a Nikon C2+ Confocal microscope coupled to NIS-elements AR software (Nikon). For yeast live cell imaging, cells were modified to endogenously express Alr1-GFP alone or endogenously express RAD52-YFP in combination with episomal Nop1-CFP, which allowed us to clearly identify cells that do not contain Rad52 foci in order to determine the percentage of cells that do actually have the foci. Cells were grown into log phase, pelleted via centrifugation, washed and resuspended in PBS before mounting onto slides or plates with a coverslip bottom for microscopy. For RNA–DNA hybrid microscopy in human cells, random fields identified by DAPI staining were captured at 100X magnification. For any given image, 7–8 2D imaging planes were acquired along the z-axis to generate 3D confocal image stacks. DAPI was used to create masks of nuclei and S9.6 intensity values for individual cells were obtained as maximum intensity planes via the NIS-elements AR (Nikon) software. Representative maximum intensity projections adjusted for background and contrast in Photoshop (Adobe) are shown.

Western blotting

For yeast, overnight cultures were diluted to 1.0×10^7 cells/ml and grown for 3 h. A total of 2.5×10^7 cells were then washed with 1 ml of cold ddH_2O. Cells were spun down at 16 000 r.c.f. at 4°C for 30 s and resuspended in 500 μl cold ddH_2O. Seventy five of Alkali/2-β-ME solution (prepared fresh by mixing 925 μl of 2N NaOH and 75 μl of 14.3 M 2-β-ME), was added and mixed by vortexing. The samples were incubated on ice for 10 min. Seventy five microliters of freshly prepared 50% TCA solution in ice-cold water was added, mixed well by vortexing and incubated on ice for 10 min then followed by centrifuging at 16 000 r.c.f. for 10 min at 4°C. Supernatant was discarded and the protein pellet resuspended in 40 μl of 1X SDS-loading buffer (128 mM Tris-HCl pH 8.8, 4X SDS loading buffer [200 mM Tris-HCl pH 6.8, 400 mM DTT, 8% SDS, 0.4% bromophenol blue, 40% glycerol], 14.3 M 2-β-ME). Samples were electrophoresed on an 8% acrylamide gel, and blotted with 1:1000 primary antibody.

RESULTS

Mg^{2+} alone or in response to CR counters R-loop buildup

In yeast, Pbp1 binds to age-related long non-coding RNA (lncRNA) molecules at the RFB and E-pro intergenic regions of *rDNA* effectively limiting R-loops harboring lncRNA-DNA hybrids (10,12,28,29). Our measurements of R-loop levels at RFB and E-pro regions via anti-RNA–DNA ChIP followed by qPCR confirm that *pbp1Δ* cells exhibit R-loop accumulation repressible by overexpression of the RNA–DNA hybrid-resolving human RNaseH1 enzyme or by subjecting cells to CR (Supplementary Figure S1A and B) (12). CR can modulate *rDNA* by activating the longevity-promoting Sir2, but CR abolishes hybrid buildup in *pbp1Δ* and *pbp1Δ sir2Δ* cells (Supplementary Figure S1B) (5,7,10,12). In fact, *sir2Δ* cells displayed some hybrid accumulation that was also abolished by CR (Supplementary Figure S1B). Instead of using Sir2, we envisioned that CR might modulate magnesium ions (Mg^{2+}) as both Pif1 and Rnh1/201 employ Mg^{2+} as a cofactor and are highly sensitive to changes in its levels (30–33). Importantly, we observed that CR increased intracellular Mg^{2+} levels by ∼20% in wild-type and *pbp1Δ* cells, where the effect was significantly compromised via deletion of the major and partly redundant Mg^{2+} transporters Alr1 and Alr2 (Figure 1A). CR boosted Mg^{2+} transporter protein levels despite down-regulating total cellular protein levels (Figure 1B, Supplementary Figure S1C). We observed similar increases in Mg^{2+} transporter transcript levels indicating that CR operates at the gene expression level (Figure 1C). Importantly, deletion of Alr1 and Alr2 additively compromised CR-dependent R-loop suppression in *pbp1Δ* cells (Figure 1D). Loss of Alr1 and/or Alr2 did not increase R-loop levels in wild-type cells (Figure 1E). In addition, we partly disrupted the ability of CR to counter R-loop buildup in *pbp1Δ* cells by lowering environmental Mg^{2+} concentration from 10 to 1 mM (Figure 1F). Our data so far reveal that CR relies on Mg^{2+} to abolish R-loop accumulation.

We next inquired if a direct environmental Mg^{2+} supplementation regimen could increase intracellular Mg^{2+} levels and counter R-loop buildup. We assessed the impact of low (50 mM), moderate (100 mM) and high (150 mM) Mg^{2+} supplementation on intracellular Mg^{2+} levels. Wild-type and *pbp1Δ* cells had similar intracellular Mg^{2+} levels under unsupplemented (10 mM) conditions but only moderate Mg^{2+} supplementation (hereafter used interchangeably with yeast Mg^{2+} supplementation or Mg^{2+}) increased intracellular Mg^{2+} levels by ∼10% irrespective of Pbp1 presence (Figure 1G). As Mg^{2+} supplementation provides more of the environmental metal for uptake by cells, we did not expect supplementation to boost Mg^{2+} transporter expression, at least not as much as CR. Indeed, relative to CR, Mg^{2+} supplementation only mildly increased Mg^{2+} transporter transcript and protein levels without altering total cellular protein levels (compare Figure 1H,I to B,C; Supplementary Figure S1C). Differences in Alr1-GFP staining

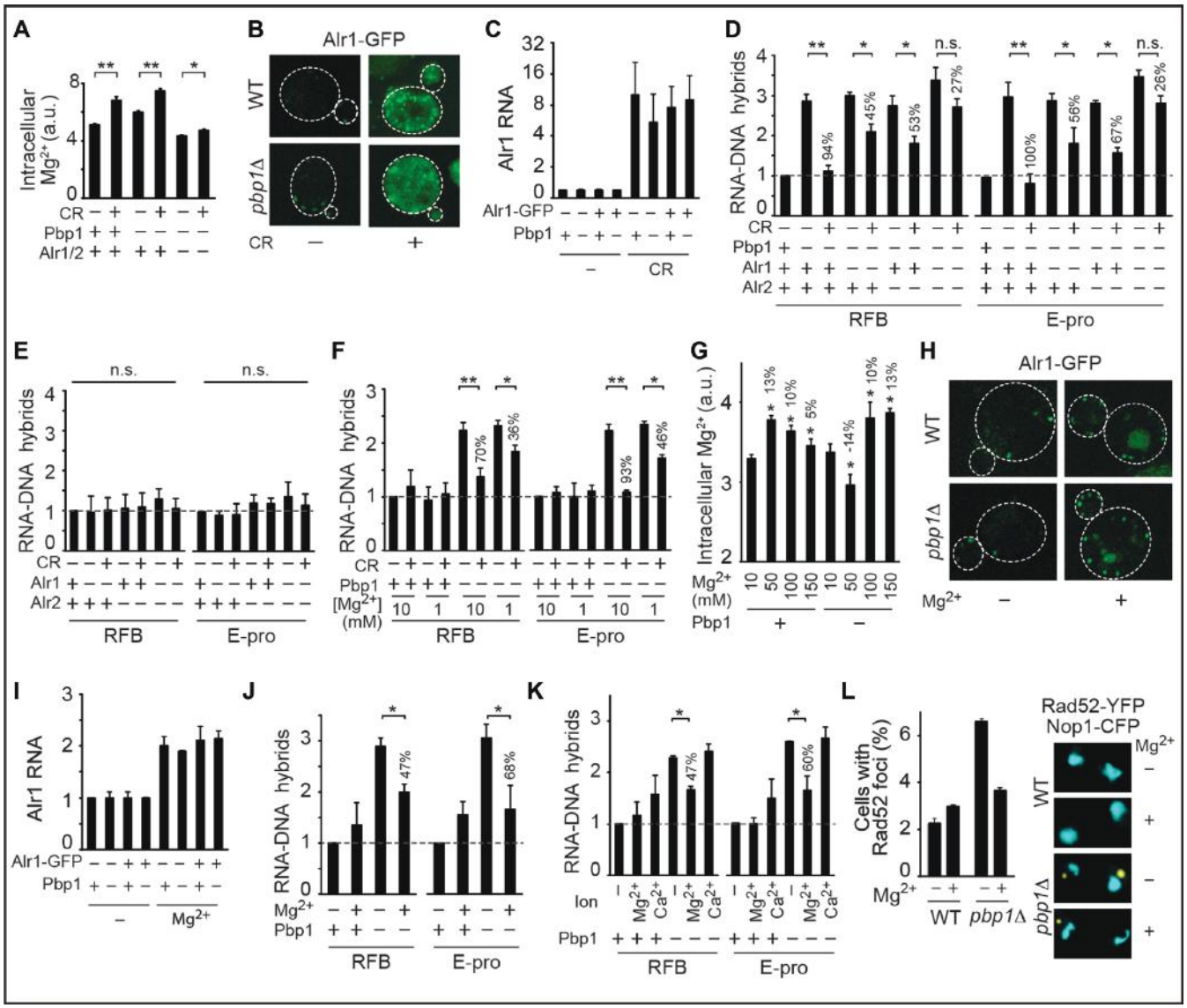

Figure 1. Mg^{2+} acting downstream or independently of calorie restriction (CR) counters R-loop accumulation. (**A**) CR increases intracellular Mg^{2+} levels and this in an Alr1/2-dependent manner. Intracellular Mg^{2+} levels were measured using MagnesiumGreen, a chemical that fluoresces upon binding to this cation (N = 3; Mean ± SD; *t*-test, $^{**}P < 0.01$, $^{*}P < 0.05$). Percentage difference relative to corresponding no Mg^{2+} treatment cells are indicated. (**B**) Confocal live cell microscopy showing that CR strongly boosts Alr1-GFP protein levels. (**C**) Reverse transcriptase PCR coupled to quantitative PCR (RT-qPCR) reveals that CR strongly induces Alr1 transcript levels regardless of GFP tagging (N = 3; Mean±SD). (**D**) Anti-RNA–DNA hybrid ChIP followed by qPCR indicates that the loss of Alr1 and Alr2 additively disrupts CR-dependent repression of R-loop buildup (N = 3; Mean ± SD; *t*-test, $^{**}P < 0.01$, $^{*}P < 0.05$, n.s. not statistically significant). Percentage difference relative to corresponding no Mg^{2+} treatment cells are indicated. (**E**) Loss of Alr1 and/or Alr2 does not alter R-loop levels in wild-type cells as revealed by anti-RNA–DNA hybrid ChIP (N = 3; Mean ± SD; n.s. not statistically significant for One-way ANOVA). (**F**) Decreasing Mg^{2+} concentration hinders the ability of CR to suppress RNA–DNA hybrid buildup (N = 3; Mean ± SD; *t*-test, $^{**}P < 0.01$, $^{*}P < 0.05$). (**G**) Effect of different Mg^{2+} supplementation regimens on intracellular Mg^{2+} levels as measured by Magnesium Green fluorescence (N = 3; Mean ± SD; **t*-test $P < 0.05$ relative to corresponding 10 mM cells). (**H**) Confocal microscopy showing that 100 mM Mg^{2+} supplementation moderately increases Alr1-GFP protein levels. (**I**) RT-qPCR reveals that 100 mM Mg^{2+} supplementation moderately induces Alr1 transcript levels regardless of GFP tagging (N = 3; Mean ± SD). (**J**) Moderate Mg^{2+} supplementation (100 mM) partly yet significantly counters RNA–DNA hybrid accumulation in *pbp1Δ* cells (N = 3; Mean ± SD; **t*-test $P < 0.05$). (**K**) A total of 100 mM Mg^{2+}, but not 100 mM Ca^{2+}, counters RNA–DNA hybrid accumulation in *pbp1Δ* cells (N = 3; Mean ± SD; **t*-test $P < 0.05$). (**L**) A total of 100 mM Mg^{2+} supplementation decreases Rad52-YFP focus formation in *pbp1Δ* cells expressing nucleolar Nop1-CFP (N = 100; Mean ± SD).

patterns are likely linked to the fact that CR is more potent than Mg^{2+} in terms of inducing transporter expression. Importantly, Mg^{2+} supplementation significantly decreased R-loop accumulation in *pbp1Δ* cells by 47% and 68% at RFB and E-pro, respectively (Figure 1J). This significant yet partial R-loop-suppressing effect of Mg^{2+} supplementation relative to that of CR is consistent with the differential increases in intracellular Mg^{2+} levels under these two environmental conditions (Figure 1A, D, G and J). Consistent with the sensitivity of Pif1 and RNaseH enzymes to changes in Mg^{2+} but not Ca^{2+} levels, Ca^{2+} supplementation failed to counter R-loop buildup (Figure 1K) (30,31). Preferential dependence of the highly conserved RNaseH enzymes on Mg^{2+} over Ca^{2+} stems from the small atomic radius and strict octahedral geometry of Mg^{2+} allowing this ion to support critical enzymatic reaction intermediates (Supplementary Figure S1D and E) (33). Importantly, the Mg^{2+} supplementation regimen used did not induce DNA damage and actually countered the elevated genome instability of *pbp1Δ* cells as detected by a decrease in the formation of DNA repair centers marked by the Rad52 repair and recombination protein (Figure 1L). Our work uncovers an Mg^{2+}-dependent pathway in which CR increases intracellular Mg^{2+} levels in order to suppress R-loop accumulation. Importantly, this Mg^{2+}-dependent process can be directly engaged in the absence of CR via direct Mg^{2+} supplementation. It is also important to note that we see changes to intracellular Mg^{2+} levels in wild-type and mutant cells under CR or Mg^{2+} supplementation conditions but the consequent benefit of countering R-loop accumulation naturally occurs in cells deficient in R-loop suppression.

R-loop suppressors are effectors of Mg^{2+}

We next aimed to investigate if the Mg^{2+}-sensitive Pif1 and Rnh1/201 do indeed fully account for R-loop suppression by Mg^{2+} supplementation. We observed that loss of Pif1 and Rnh1/201 additively and fully abrogated Mg^{2+}-dependent suppression of R-loop accumulation in *pbp1Δ* cells but was ineffectual in wild-type cells (Figure 2A and B). Loss of Pif1 and/or Rnh1/201 did not lead to any R-loop accumulation in wild-type cells (Figure 2A and B). In addition, Mg^{2+}-dependent repression of R-loop buildup was unaltered in cells lacking Sir2 or Fob1, which respectively mediate chromatin silencing and replication fork blocking at *rDNA* (Figure 2C) (10,34). Moreover, Mg^{2+} failed to alter enrichments of RNA Polymerase II (RNA Pol II) or the open chromatin mark diAcH3K9/14 (histone H3 acetylated at lysines 9 and 14) regardless of Pbp1 or Pif1/Rnh1/201 status (Figure 2D and E) (23). Yeast Sen1, the ortholog of human SENATAXIN, is an RNA–DNA hybrid helicase whose enzymatic function at yeast rDNA coordinates hybrid resolution and early transcriptional termination of rDNA lncRNA (17,35). In fact, decreases and increases in Sen1 activity respectively lead to increases and decreases in RNA Pol II levels at the studied loci (17,35). In contrast, Mg^{2+} supplementation did not alter RNA Pol II localization within our experimental conditions (Figure 2D), indicating that Sen1 is not implicated in Mg^{2+}-dependent R-loop suppression.

Mg^{2+} also did not decrease lncRNA levels in *pbp1Δ* cells arguing against Mg^{2+}-dependent R-loop repression being a reflection of decreased RNA availability for R-loop formation (Figure 2F). In fact, as expected if Mg^{2+}-dependent R-loop resolution frees lncRNAs from hybrids, we found that Mg^{2+} generally increased free lncRNA levels (Figure 2F). Dependence of Mg^{2+} on Pif1 and Rnh1/201 cannot be explained by changes in cellular growth rates (Supplementary Figure S2A). Our findings reveal that Pif1 and Rnh1/201 additively and fully account for the ability of Mg^{2+} to counter R-loop buildup independently of controlling RNA Pol II, chromatin, replication, RNA turnover and overall cellular growth. Despite the total loss of R-loop suppression by Mg^{2+} in the absence of Pif1 and Rnh1/201, future work should still examine if additional Mg^{2+}-responsive factors may also contribute in a more accessory role.

Next, we asked if Mg^{2+} supplementation overlaps with CR-induced remodeling of metabolism and if direct glycolytic constriction without environmental CR would counter R-loop accumulation redundantly with Mg^{2+} supplementation (4,5). Our analysis showed Mg^{2+} supplementation increasing expression of 60% of top CR-inducible metabolic genes in wild-type and *pbp1Δ* cells (Supplementary Figure S2B) (4). Half of those Mg^{2+}-responsive genes were induced to a similar extent, while the other half was more responsive to CR. This suggests the existence of a substantial and unexpected overlap between CR and Mg^{2+} homeostasis. Hexokinase 2 (Hxk2) is an enzyme that phosphorylates glucose in preparation for glycolysis and *hxk2Δ* cells experience a glycolytic constriction effect that essentially mimics metabolic responses to environmental CR (4). Importantly, we found that *hxk2Δ* was redundant with Mg^{2+} supplementation in decreasing R-loop accumulations in *pbp1Δ* cells (Figure 2G) (5). We conclude that CR-induced metabolic constriction and direct Mg^{2+} supplementation induce overlapping processes including R-loop accumulation-suppressing Mg^{2+}-dependent processes. Future studies in the field should assess how many of the numerous effects of CR involve or reflect increased Mg^{2+} levels.

We also aimed to test if we can abolish the relative R-loop-suppressing effect of Mg^{2+} by overexpressing the R-loop/G4DNA-stabilizing factor Stm1 (12,24). As predicted, overexpression of Stm1 in *pbp1Δ* cells further increased R-loop levels by ∼25% (Figure 2H). Unexpectedly, the Mg^{2+}-dependent relative decrease in R-loop levels was 73% and 57% in *pbp1Δ* cells with and without Stm1 overexpression, respectively (Figure 2H) (12,24). Despite this increased relative ability of Mg^{2+} to repress R-loops in *pbp1Δ* cells overexpressing Stm1, there remained in these cells an Mg^{2+}-resistant fraction of R-loops similar to that seen in *pbp1Δ* cells without Stm1 overexpression. These findings suggest that certain biochemical features of such an Mg^{2+}-resistant fraction may underlie this resistance rather than our Mg^{2+} supplementation regimen reaching its maximal R-loop-suppressing capacity. Our findings also suggest that environmental CR likely triggers additional Mg^{2+}-independent processes to fully abolish even Mg^{2+}-resistant R-loop fractions (compare Figures 1D and 2A). Such Mg^{2+} independent processes are unlikely to require transcrip-

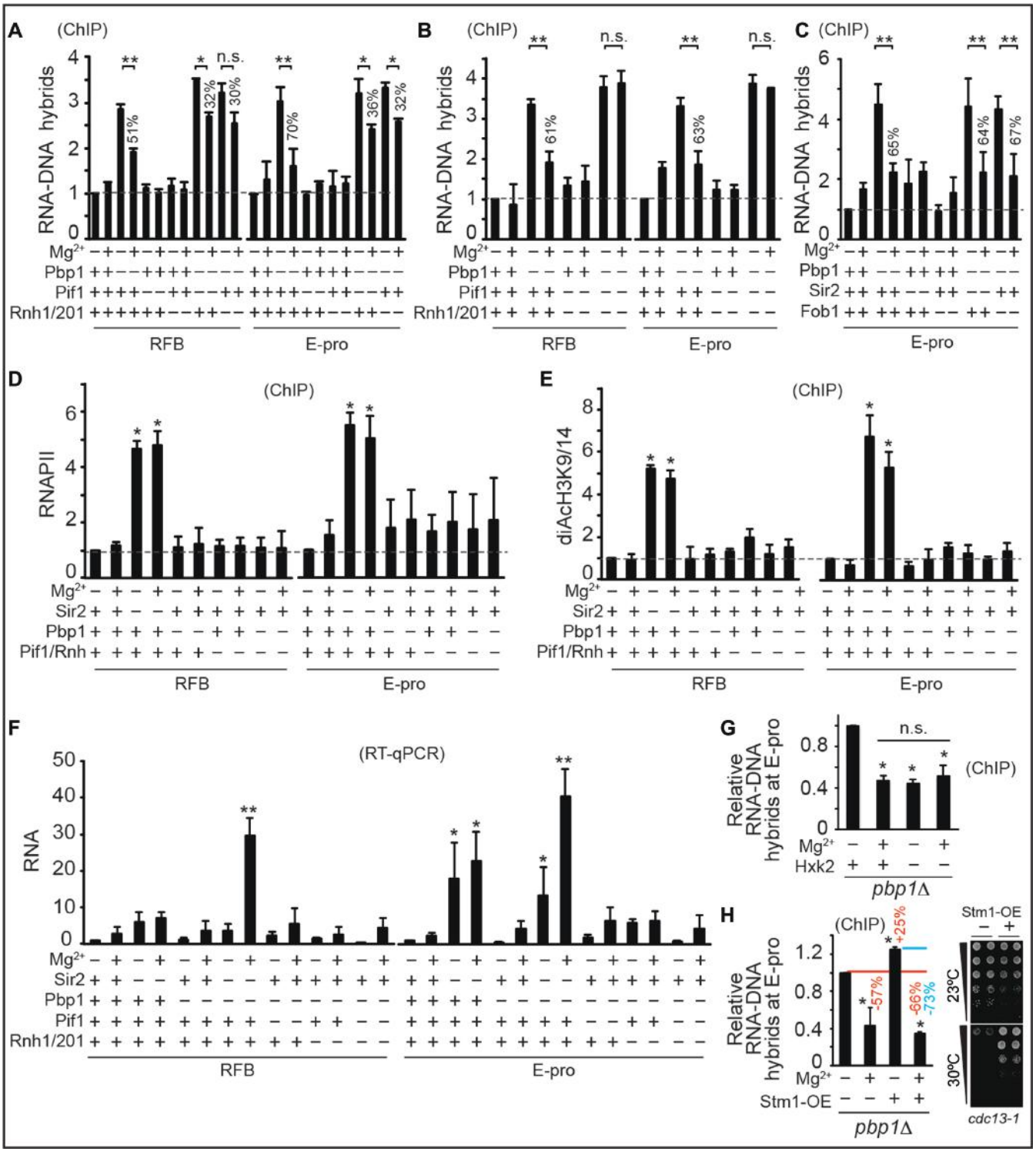

Figure 2. Mg^{2+} acts specifically via suppressors of R-loops to counter their accumulation. (**A** and **B**) Mg^{2+} supplementation requires Mg^{2+}-sensitive Pif1 and Rnh1/201 to counter RNA–DNA hybrid accumulation. (**C**) Sir2 and Fob1 are dispensable for Mg^{2+}-dependent suppression of RNA–DNA hybrid buildup. (**D** and **E**) Mg^{2+} supplementation does not alter the enrichment of RNA Pol II or diAcH3K9/14. Rnh symbolizes Rnh1/201. Control is *sir2Δ*. (**F**) Mg^{2+} does not decrease free long non-coding RNA (lncRNA) levels but can increase it especially in *pbp1Δ sir2Δ* cells. (**G**) Glycolytic constriction via *hxk2Δ* and Mg^{2+} supplementation redundantly suppress R-loop accumulation. (**H**) Mg^{2+} efficiently suppresses R-loops hyper-stabilized via Stm1 overexpression (left). Overexpressed Stm1 is functional as shown by rescue of *cdc13-1* cell growth at 30°C (right). (**A**–**H**) Graphs show N = 3, Mean ± SD and *t*-test, $^{**}P < 0.01$, $^{*}P < 0.05$, n.s. not statistically significant.

tional silencing as CR fully suppresses hybrid buildup in *pbp1Δ* cells even in the absence of Sir2 (Supplementary Figure S1B). Other non-mutually exclusive possibilities are that specific chromatin modifications or that the greater increases in intracellular Mg^{2+} levels under environmental CR conditions may allow it to resolve all R-loops.

Mg^{2+}-responsiveness of R-loop suppressors restores genome stability

We next wanted to test if Mg^{2+} physically targets R-loop suppressors to R-loop accumulating *rDNA* loci and decipher the impact of such a potential localization on *rDNA* stability and cellular longevity.

We found Pif1 and Rnh1/201 to be physically enriched at the RFB and E-pro regions of *pbp1Δ* cells under Mg^{2+} supplementation conditions (Figure 3A). Despite this increased physical targeting to R-loop accumulating loci, the levels of these R-loop-suppressing proteins were unaltered by Mg^{2+} (Supplementary Figure S3A). We note that Pbp1 loss was sufficient to target Pif1 to these R-loop accumulating regions whereas Rnh1 targeting additionally required Mg^{2+} supplementation (Figure 3A). These findings indicate that both types of R-loop-repressing enzymes are physically located at R-loop accumulating *rDNA* loci in the presence of Mg^{2+} supplementation. Differential requirements for Pif1 and Rnh1/201 responses indicate that not all R-loop suppressors are the same. More importantly, our results establish a direct physical link between R-loop suppressors and the R-loop-accumulating loci they regulate in the presence of increased Mg^{2+}.

R-loop buildup in *pbp1Δ* cells stalls *rDNA* replication increasing a form of genome-destabilizing aberrant recombination called USCE without disrupting global DNA replication dynamics (Figure 3B, Supplementary Figure S3B and Table S1) (8,12). Consistent with the observation that the localization of Pif1, but not Rnh1, is increased at R-loop accumulating loci in unsupplemented *pbp1Δ* cells, we observed that *pbp1Δ pif1Δ* cells, but not *pbp1Δ rnh1/201Δ* cells exhibited higher USCE relative to *pbp1Δ* cells (Figure 3B). Mg^{2+} significantly decreased USCE in *pbp1Δ* (46%), *pbp1Δ pif1Δ* (35%) and *pbp1Δ rnh1/201Δ* (32%) cells, but did not affect *pbp1Δ pif1Δ rnh1/201Δ* cells (Figure 3B). Mg^{2+} supplementation also decreased erroneous rDNA replication fork blocks typically observed in *pbp1Δ* cells (Supplementary Figure S3C). Thus, Mg^{2+} requires Pif1 and Rnh1/201 to counter R-loop-induced aberrant recombination.

We also tested if *rDNA* stabilization by Mg^{2+} is specific to R-loop repression. Stm1 promotes R-loop accumulation at *rDNA* in *pbp1Δ* cells (12). We reasoned that if Mg^{2+} increases *rDNA* stability independently of R-loop suppression, Mg^{2+} supplementation would still cause a similar relative decrease in *rDNA* instability in both *pbp1Δ* and *pbp1Δ stm1Δ* cells. Deletion of Stm1 in *pbp1Δ* cells increased *rDNA* stability and Mg^{2+} triggered a relative decrease in *rDNA* instability in *pbp1Δ* but not *pbp1Δ stm1Δ* cells (Figure 3C). Mg^{2+} supplementation slightly but significantly increased rDNA USCE in *stm1Δ* cells suggesting that some low levels of hybrids may be beneficial and that excessive hyper-suppression of hybrids may mildly increase rDNA instability (Figure 3C). Our findings indicate that Mg^{2+} restores *rDNA* stability by specifically repressing R-loop buildup.

Instability at *rDNA* as in *pbp1Δ* cells shortens replicative lifespan that is defined by the number of times that a yeast mother cell replicates its DNA and yields progeny before senescence (Figure 3D, Supplementary Table S2) (8,26,29,36). We found that Mg^{2+} supplementation increases the lifespan of *pbp1Δ*, *pbp1Δ pif1Δ*, *pbp1Δ rnh1/201Δ*, but not *pbp1Δ pif1Δ rnh1/201Δ* cells (Figure 3D, E, F and G; Supplementary Table S2). Failure of Mg^{2+} to increase the lifespan of *pbp1Δ pif1Δ rnh1/201Δ* cells is not due to the shorter lifespan of these cells as Mg^{2+} successfully increased the very short lifespan of cells lacking Npl3, another RNA-binding R-loop suppressor (Supplementary Figure S3D) (37). More importantly, by combining Mg^{2+} supplementation with global R-loop destabilization via *stm1Δ*, we extended the lifespan of *pbp1Δ* cells beyond that of wild-type cells (Figure 3H). Our results demonstrate that Mg^{2+}-driven repression of DNA-destabilizing R-loop accumulation can increase or even help extend lifespan.

Mg^{2+}-dependent repression of R-loop accumulation is evolutionarily conserved

ATXN2, the human ortholog of yeast Pbp1, physically associates to hundreds of transcripts in human cells (38). If ATXN2 counters R-loops is unknown but ATXN2 dysfunction leads to severely debilitating and often lethal neurodegenerative diseases called amyotrophic lateral sclerosis (ALS) and spinocerebellar ataxia-2 (SCA2) (39,40). In addition, we previously hypothesized that R-loop regulation may link many ALS-associated genes to each other (15).

First, we aimed to study the natural localization of ATXN2 relative to R-loop signal distribution inside the cell nucleus. Immunofluorescence analysis revealed that endogenous ATXN2 localizes to hundreds of small foci in the nucleus and cytoplasm but displays a primary localization to a handful of larger nuclear foci identified as nucleoli via co-localization with nucleolar markers (Figure 4A, B, Supplementary Figure S4A and B). Co-labeling revealed an inverse correlation for ATXN2 and R-loops in the nucleoplasm and nucleoli (Figure 4A). Importantly, anti-R-loop immunofluorescence followed by single cell analysis revealed that knockdown of human ATXN2 results in a highly significant nuclear R-loop accumulation (Figure 4C, Supplementary Figure S4C). Nuclear increases were observed in both the nucleolus and nucleoplasm (Figure 4C). Over expression of the RNA–DNA hybrid suppressor human RNaseH1, but not empty vector control, significantly countered nuclear R-loop accumulation in ATXN2-deficient cells (Figure 4D and E). Thus, similar to yeast Pbp1, loss of human ATXN2 triggers nuclear R-loop accumulation.

We next asked if supplementing human cells with Mg^{2+} suppresses aberrant R-loop accumulation and promotes genome stability. Titration experiments revealed that 10 mM Mg^{2+} supplementation countered R-loop accumulation in ATXN2-deficient cells without altering ATXN2 knockdown efficiency or ATXN2 localization (Figure 5A and B). Mg^{2+} supplementation regimens higher than 10

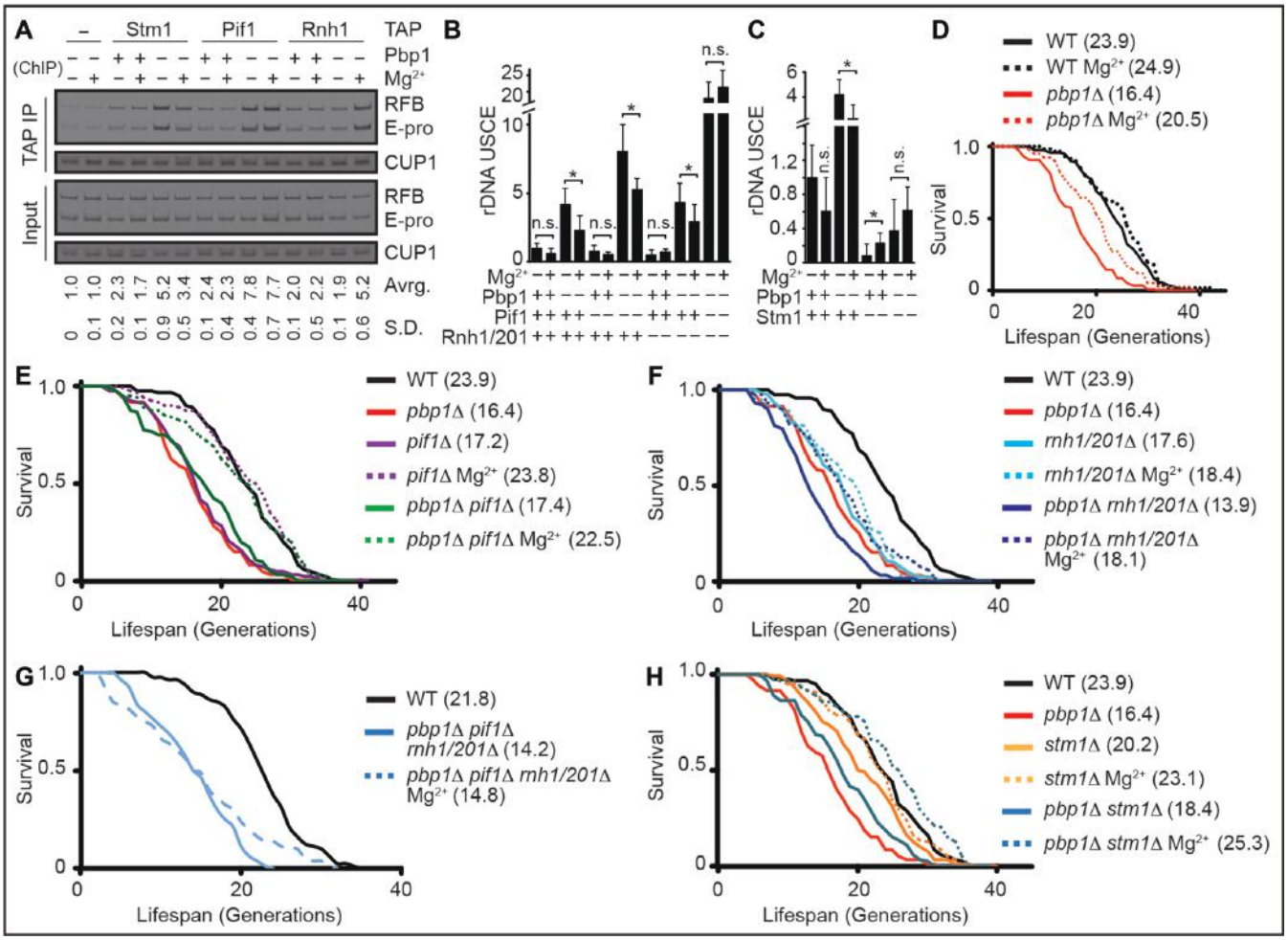

Figure 3. Mg^{2+} increases rDNA stability and cellular lifespan by countering R-loop buildup. (**A**) TAP-tagged Pif1 and Rnh1 are physically located at R-loop-accumulating *rDNA* loci in *pbp1Δ* cells under Mg^{2+} supplementation. R-loop-stabilizing/enriched Stm1-TAP control is included and relative fold enrichments (Mean ± SD) for RFB and E-pro are shown below gels. (**B**) Mg^{2+} counters deleterious *rDNA* USCE in *pbp1Δ* cells by operating via Pif1 and Rnh1/201. (**C**) Mg^{2+} supplementation does not decrease *rDNA* USCE in *pbp1Δ* cells lacking the R-loop stabilizer Stm1. (**B** and **C**) Shown are rates (N = 5000–25 000; Mean ± SD) and *t*-test $*P < 0.05$ with full data and statistics in Supplementary Table S1. Not statistically significant indicated by n.s. (**D–G**) Mg^{2+} supplementation increases the replicative lifespan of cells lacking (**D**) Pbp1, even in the absence of (**E**) Pif1 or (**F**) Rnh1/201, (**G**) but not both. (**H**) Combining Mg^{2+} supplementation with *stm1Δ* extends the replicative lifespan of *pbp1Δ* cells. (**D–H**) Shown are replicative lifespan curves and mean lifespans (N = 80) in parentheses with full data and Wilcoxon's rank-sum test statistics in Supplementary Table S2.

mM did not confer increased R-loop suppression and actually exhibited elevated toxicity above 50 mM (not shown). Importantly, ATXN2 deficient cells exhibited elevated levels of the DNA damage marker γH2AX (Figure 5C). This elevated genome instability was significantly decreased upon 10 mM Mg^{2+} supplementation (Figure 5C). Thus, an Mg^{2+} supplementation regimen (10 mM) less substantial than that used in our yeast experiments (100 mM) efficiently counters R-loop accumulation and genome instability in ATXN2-deficient human cells.

Based on the knowledge gained from our work in yeast, we next set out to identify the mechanistic requirements for Mg^{2+} to counter human R-loop accumulation. We found that RNaseH1 knockdown abolished Mg^{2+}-dependent suppression of R-loop accumulation (Figure 5D and E). PIF1 deficiency did not compromise R-loop repression by Mg^{2+} despite globally decreasing R-loop levels likely due to compensation by other R-loop suppressors (Figure 5D). On another front, ALS patients from Guam, a Territory of the United States located in the northwestern Pacific Ocean, carry mutations in the TRPM7 Mg^{2+} transporter (41). Knockdown of TRPM7 in ATXN2-deficient cells did not alter R-loop levels but disrupted R-loop repression by Mg^{2+} (Figure 5F and G). Knockdown of the ALS-unrelated control MAGT1 Mg^{2+} transporter in ATXN2-deficient cells actually lowered R-loop levels likely due to confounding compensation by other Mg^{2+} transporters in the cell (Figure 5F). As a potentially similar compensation is not seen when we knockdown TRPM7, this highlights a potentially unique role for TRPM7 in Mg^{2+}-dependent human R-loop repression (Figure 5F). We note that unlike yeast Alr1/2, transcript levels of the Mg^{2+} transporter TRPM7 were already elevated in ATXN2 deficient cells regardless of Mg^{2+} supplementation, indicating the existence of genetic interactions between ATXN2 and Mg^{2+} homeostasis in human cells (Figure 5F and G). Cells deficient in RNaseH1 or

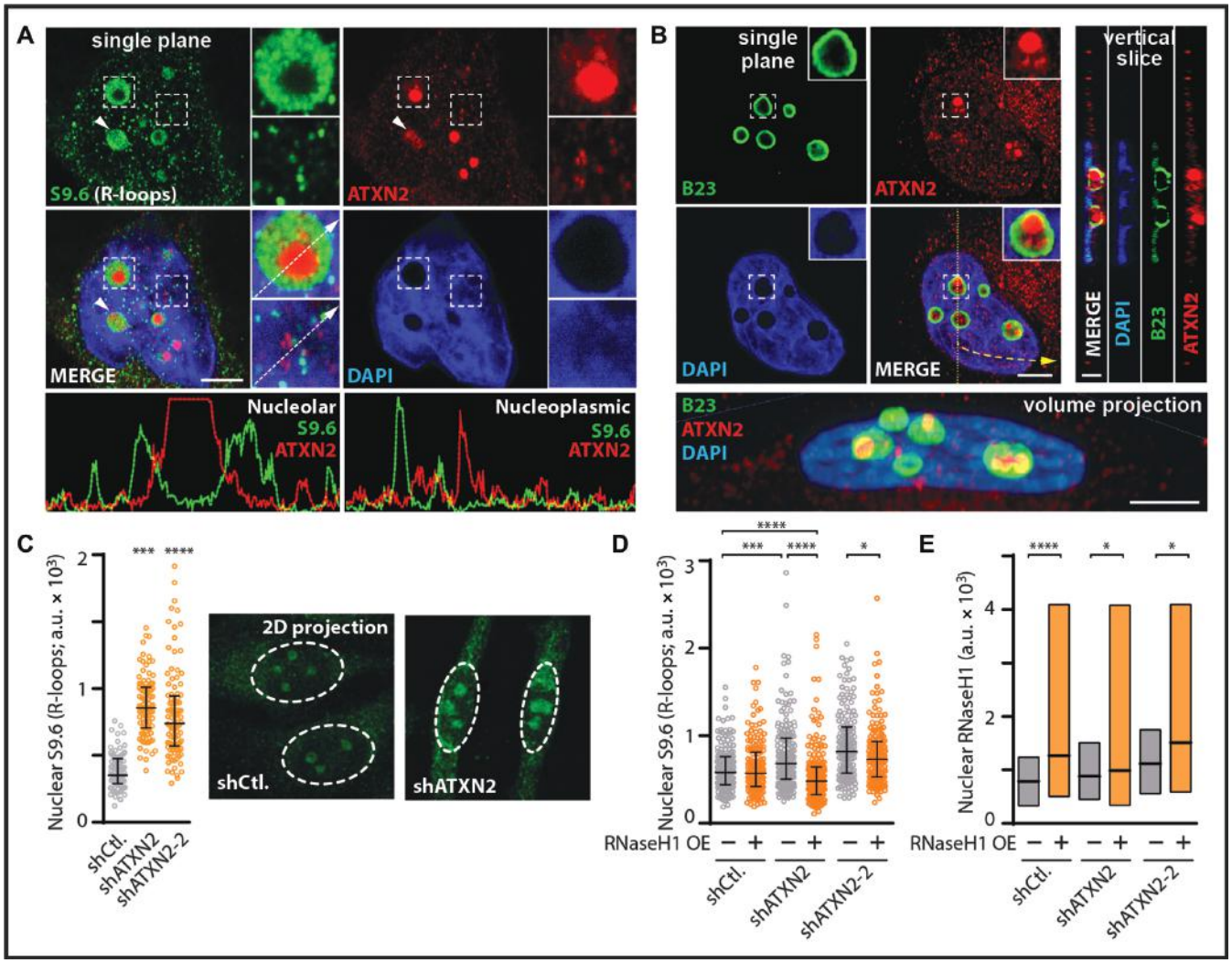

Figure 4. Human ATXN2 deficiency triggers nuclear R-loop accumulation. (**A**) Double immunofluorescence coupled to confocal microscopy reveals an inverse correlation for RNA–DNA hybrid and ATXN2 signals in HeLa cells. DAPI-stained DNA and single plane images are shown. Dashed squares outline areas shown in zoom inset images. Arrowheads highlights inverse localization of ATXN2 and R-loops even in a single nucleolus. Intensity plots below the images are for nucleolar and nucleoplasmic regions along the path of the white arrows in inset images. Bar, 5 μm. (**B**) Double immunofluorescence and confocal microscopy reveal that major ATXN2 foci are located within B23-outlined nucleoli of HeLa cells. DAPI-stained DNA as well as single plane, vertical slice and volume views are shown. Bar, 5 μm. (**C**) Short hairpin RNA (shRNA)-mediated stable knockdown of ATXN2 in HeLa cells resulted in R-loop accumulation as revealed by anti-RNA–DNA hybrid immunofluorescence and quantification of 2D images obtained by projecting confocal stacks onto a single plane. Shown are representative 2D projection images with quantification presented as a scatter plot to better capture cell population data (N = 150 per condition; Mean ± Quartiles; $^{****}P < 0.0001$, $^{***}P < 0.001$ for the Mann–Whitney test). (**D**) Overexpression of human RNaseH1 (+), but not empty vector control (−), counters R-loop accumulation in shATXN2 HeLa cells as revealed by anti-RNA–DNA hybrid immunofluorescence (N = 150 per condition; Mean ± Quartiles; $^{****}P < 0.0001$, $^{***}P < 0.001$, $^{*}P < 0.05$ for the Mann–Whitney test). (**E**) Quantification analysis of nuclear signal from anti-RNaseH1 immunofluorescence indicating that overexpression of RNaseH1 (+), but not empty vector control (−), increases RNaseH1 protein levels in shCtl. and shATXN2 HeLa cells (N = 150 per condition; Mean ± Quartiles; $^{****}P < 0.0001$, $^{*}P < 0.05$ for the Mann–Whitney test).

TRPM7 alone did not exhibit significant R-loop accumulations in our assays (not shown). We also successfully used Mg^{2+} to decrease R-loop buildup in cells deficient in the R-loop-repressing BRCA2 tumor suppressor indicating that Mg^{2+} can counter R-loop accumulations triggered by the loss of other disease-linked R-loop suppressors (Figure 5H and I) (42). We conclude that Pbp1/ATXN2 and Mg^{2+} supplementation acting via Mg^{2+} transporters, RNaseH enzymes and potentially other Mg^{2+}-sensitive factors such as Pif1 counter deleterious R-loop accumulation in yeast and human cells evolutionary separated by over a billion years.

DISCUSSION

Our work uncovers a conserved Mg^{2+}-dependent pathway that acts alone or in response to calorie restriction to counter deleterious RNA–DNA hybrids or R-loops (Figure 6). We propose that direct Mg^{2+} supplementation, which can engage this pathway, offers a simple and effective approach to counter genome-destabilizing R-loop buildup pertinent to different human diseases. The herein identified components of this pathway, including Mg^{2+} transporters and R-loop suppressors, also constitute novel targets for the development of future therapeutics focusing on the sup-

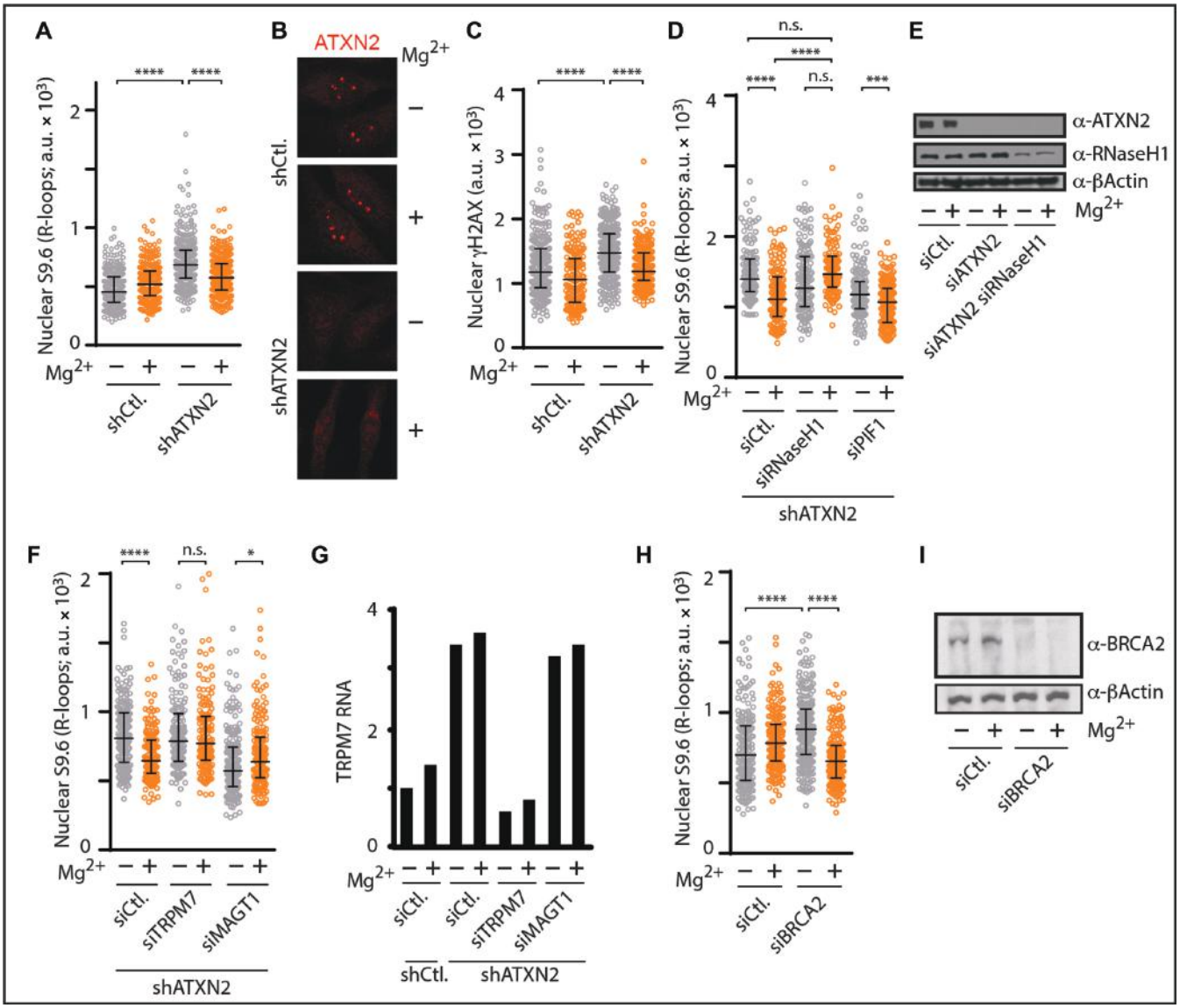

Figure 5. Mg^{2+} counters human R-loop accumulation by relying on RNaseH1 and the TRPM7 Mg^{2+} transporter. (**A**) Anti-RNA–DNA hybrid immunofluorescence indicates that 10 mM Mg^{2+} supplementation significantly decreases nuclear R-loop buildup in shATXN2 HeLa cells as shown in the scatter plot to better represent cell population data (N = 150 per condition; Mean ± Quartiles; ****$P < 0.0001$ for the Mann–Whitney test). (**B**) Representative anti-ATXN2 immunofluorescence images from cells transiently transfected with siCtl. or siATXN2 in the presence or absence of 10 mM Mg^{2+} supplementation. Note how Mg^{2+} supplementation does not alter ATXN2 levels or localization. (**C**) Anti-γH2AX immunofluorescence imaging and quantitation indicate that 10 mM Mg^{2+} supplementation counters γH2AX accumulation in shATXN2 HeLa cells (N = 150 per condition; Mean ± Quartiles; ****$P < 0.0001$ for the Mann–Whitney test). (**D**) Anti-RNA–DNA hybrid immunofluorescence reveals that transient knockdown of RNaseH1, but not PIF1, abolishes the R-loop-suppressing effect of 10 mM Mg^{2+} supplementation in shATXN2 HeLa cells (N = 150 per condition; Mean ± Quartiles; ****$P < 0.0001$, ***$P < 0.001$ for the Mann–Whitney test; n.s. not statistically significant). (**E**) Immunoblots showing transient knockdown of RNaseH1 in ATXN2-deficient HeLa cells. Anti-β-Actin immunoblotting served as loading control. (**F**) Anti-RNA–DNA hybrid immunofluorescence reveals that transient knockdown of TRPM7, but not MAGT1, abolishes the R-loop-suppressing effect of 10 mM Mg^{2+} supplementation in shATXN2 HeLa cells (N = 150 per condition; Mean ± Quartiles; ****$P < 0.0001$, *$P < 0.05$ for the Mann–Whitney test; n.s. not statistically significant). (**G**) RT-qPCR measuring TRPM7 RNA levels reveals that TRPM7 and MAGT1 RNA levels are unexpectedly already increased in shATXN2 HeLa cells and illustrates the efficacy of siTRPM7 in our knockdown experiments. (**H**) Anti-RNA–DNA hybrid immunofluorescence indicates that 10 mM Mg^{2+} supplementation counters nuclear R-loop buildup in siBRCA2 HeLa cells (N = 150 per condition; Mean ± Quartiles; ****$P < 0.0001$ for the Mann–Whitney test). (**I**) Immunoblots confirming the efficacy of siRNA-mediated BRCA2 knockdown. Anti-β-Actin immunoblotting served as loading control.

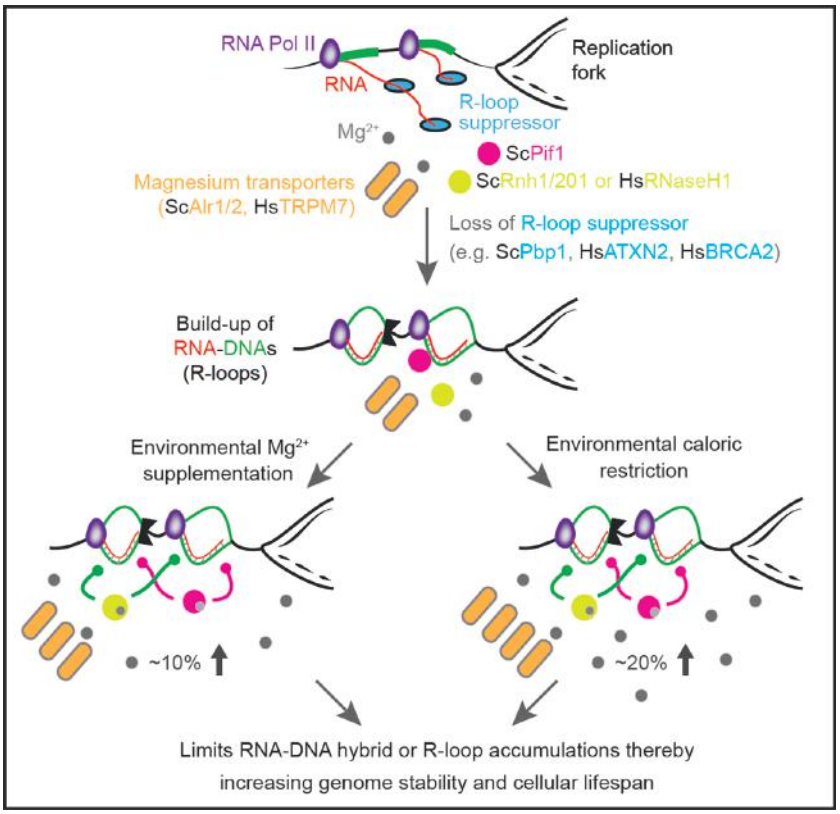

Figure 6. Evolutionarily conserved Mg^{2+}-dependent process alone or in response to calorie restriction suppresses genome-destabilizing RNA–DNA hybrids, or R-loops. Loss of conserved factors such as yeast Pbp1 or human ATXN2 leads to the accumulation of genome-destabilizing RNA–DNA hybrids. Environmental calorie restriction or direct and measured Mg^{2+} supplementation (100 mM in yeast; 10 mM in human) increases intracellular Mg^{2+} levels thereby engaging Mg^{2+}-sensitive R-loop suppressors (e.g. yeast Pif1 and Rnh1/201 or human RNaseH1) allowing them to counter R-loop accumulation and restore genome stability and cellular lifespan. Sc, *S. cerevisiae*; Hs, *H. sapiens*.

pression of deleterious R-loop accumulation. As many cellular processes are Mg^{2+} sensitive, we expect that elevated intracellular Mg^{2+} levels, especially under calorie restriction, may modulate pathways unrelated to R-loop control (43). Thus, future work should assess the potentially broad impact of increased Mg^{2+} levels especially under calorie restriction. This should include a detailed characterization of the potential impact of magnesium on metabolic processes in both the nucleus and cytoplasm.

Despite the potentially wide impact of Mg^{2+}, our findings indicate that rDNA-stabilization by Mg^{2+} is specific to its role in R-loop suppression. First, Mg^{2+}-dependent R-loop repression and rDNA stabilization is additively and fully abolished in the absence of Pif1 and Rnh1/201. Second, that Mg^{2+} but not Ca^{2+} counters R-loop buildup is consistent with the structure and function of these R-loop suppressing enzymes. Third, Mg^{2+}-sensitive R-loop suppressors are directly detected at R-loop-accumulating loci under Mg^{2+} supplementation conditions. Fourth, Mg^{2+} did not alter local chromatin, RNA Pol II or lncRNA features at sites where R-loop repression is observed. Fifth, the relative stabilization of rDNA by Mg^{2+} is fully lost if R-loops are already independently destabilized via Stm1 deletion. In addition, consistent with our observations, a recent study identified specific roles for Mg^{2+} in cellular timekeeping (44). Overall, we find that Mg^{2+}, much like hydrogen ions, can elicit specific biological responses.

We do observe similarities and differences between CR and Mg^{2+} supplementation in yeast. Common features include dependence on Mg^{2+}-sensitive R-loop suppressors and increases in Mg^{2+} levels. Main differences are that CR more substantially increases intracellular Mg^{2+} levels and completely abolishes R-loop accumulation. Despite these distinctions, the level of R-loop repression that we observe correlates very well with changes in intracellular Mg^{2+} levels. CR in *pbp1Δ* cells, Mg^{2+} supplementation in *pbp1Δ* cells and CR in *pbp1Δ alr1Δ alr2Δ* cells triggers a 20%, 10% and 6% increase in intracellular Mg^{2+} levels matched by a 90–100%, 50–70% and 25% decrease in R-loop levels, respectively.

In humans, R-loop repression is emerging as a central function for various disease-linked gene products including ATXN2 (yeast Pbp1; ALS and SCA2; shown here), SETX (yeast Sen1; ALS and occulomotor apraxia type 2 (AOA2)), BRCA1/2 (breast/ovarian cancer), RNaseH2 (yeast Rnh201; Aicardi-Goutières Syndrome) and PIF1 (yeast Pif1; cellular transformation) (15,20,39,42,45–53). Mutations in the TRPM7 Mg^{2+} transporter are found in ALS patient populations (41). We propose that direct Mg^{2+} supplementation should be considered as an option to

counter R-loop accumulation pertinent to several human diseases.

Taken together, our findings identify Mg^{2+} as a biochemical signal of beneficial calorie restriction, establish Mg^{2+} as an R-loop suppressing biological metal, and indicate that Mg^{2+} supplementation should be considered for patients suffering from various R-loop accumulation-linked diseases.

SUPPLEMENTARY DATA

Supplementary Data are available at NAR Online.

ACKNOWLEDGEMENTS

The authors thank J. Greenblatt, D. Durocher, M. Ohh (Toronto, Canada) and D. Moazed (Harvard, USA) for discussions and comments on the paper.
Author Contributions: Conception, J.S.S. and K.M.; writing, K.J.A. and K.M.; text editing and westerns, J.N.Y.C.; Yeast strains, J.S.S., B.H., A.H., E.V., S.A.K.; Mg^{2+} measurements, J.S.S.; ChIP, J.S.S., J.N.Y.C.; USCE, J.S.S., E.V., N.X.L.; Lifespan, J.S.S., R.G., S.A.K.; Microscopy, K.J.A., J.S.S.; Growth assays, J.S.S.; RT-qPCR, J.N.Y.C; DNA combing, B.H., G.W.B.; Structure, J.E.L.

FUNDING

Canadian Institutes of Health Research (CIHR) Vanier Doctoral Awards [to K.J.A. and J.S.S.]; Canadian Institutes of Health Research (CIHR) and Canada Research Chair [CIHR-299429 and Canada Research Chair-950230661 to K.M.]; Canadian Institutes of Health Research (CIHR) and Canadian Cancer Society Research Institute [CIHR-MOP79368 and Canadian Cancer Society Research Institute-702310 to G.W.B.]. Funding for open access charge: CIHR-299429.
Conflict of interest statement. MaRS Innovation (Toronto) did not fund this work but K.M., K.J.A., J.N.Y.C. and J.S.S. have signed a preliminary agreement with this organization and the University of Toronto to develop and commercialize intellectual property related to this study.

REFERENCES

1. Dillin,A., Gottschling,D.E. and Nystrom,T. (2014) The good and the bad of being connected: The integrons of aging. *Curr. Opin. Cell Biol.*, **26**, 107–112.
2. Szafranski,K. and Mekhail,K. (2014) The fine line between lifespan extension and shortening in response to caloric restriction. *Nucleus*, **5**, 56–65.
3. Kaeberlein,M., Rabinovitch,P.S. and Martin,G.M. (2015) Healthy aging: The ultimate preventative medicine. *Science*, **350**, 1191–1193.
4. Lin,S.J., Kaeberlein,M., Andalis,A.A., Sturtz,L.A., Defossez,P.A., Culotta,V.C., Fink,G.R. and Guarente,L. (2002) Calorie restriction extends Saccharomyces cerevisiae lifespan by increasing respiration. *Nature*, **418**, 344–348.
5. Lin,S.J., Defossez,P.A. and Guarente,L. (2000) Requirement of NAD and SIR2 for life-span extension by calorie restriction in Saccharomyces cerevisiae. *Science*, **289**, 2126–2128.
6. Kaeberlein,M., Powers,R.W. 3rd, Steffen,K.K., Westman,E.A., Hu,D., Dang,N., Kerr,E.O., Kirkland,K.T., Fields,S. and Kennedy,B.K. (2005) Regulation of yeast replicative life span by TOR and Sch 9 in response to nutrients. *Science*, **310**, 1193–1196.
7. Imai,S., Armstrong,C.M., Kaeberlein,M. and Guarente,L. (2000) Transcriptional silencing and longevity protein Sir2 is an NAD-dependent histone deacetylase. *Nature*, **403**, 795–800.
8. Kaeberlein,M., McVey,M. and Guarente,L. (1999) The SIR2/3/4 complex and SIR2 alone promote longevity in Saccharomyces cerevisiae by two different mechanisms. *Genes Dev.*, **13**, 2570–2580.
9. Ide,S., Miyazaki,T., Maki,H. and Kobayashi,T. (2010) Abundance of ribosomal RNA gene copies maintains genome integrity. *Science*, **327**, 693–696.
10. Mekhail,K. and Moazed,D. (2010) The nuclear envelope in genome organization, expression and stability. *Nat. Rev. Mol. Cell Biol.*, **11**, 317–328.
11. Jack,C.V., Cruz,C., Hull,R.M., Keller,M.A., Ralser,M. and Houseley,J. (2015) Regulation of ribosomal DNA amplification by the TOR pathway. *Proc. Natl. Acad. Sci. U.S.A.*, **112**, 9674–9679.
12. Salvi,J.S., Chan,J.N., Szafranski,K., Liu,T.T., Wu,J.D., Olsen,J.B., Khanam,N., Poon,B.P., Emili,A. and Mekhail,K. (2014) Roles for Pbp1 and caloric restriction in genome and lifespan maintenance via suppression of RNA-DNA hybrids. *Dev. Cell*, **30**, 177–191.
13. Santos-Pereira,J.M. and Aguilera,A. (2015) R loops: New modulators of genome dynamics and function. *Nat. Rev. Genet.*, **16**, 583–597.
14. Duquette,M.L., Handa,P., Vincent,J.A., Taylor,A.F. and Maizels,N. (2004) Intracellular transcription of G-rich DNAs induces formation of G-loops, novel structures containing G4 DNA. *Genes Dev.*, **18**, 1618–1629.
15. Salvi,J.S. and Mekhail,K. (2015) R-loops highlight the nucleus in ALS. *Nucleus*, **6**, 23–29.
16. Houseley,J., Kotovic,K., El Hage,A. and Tollervey,D. (2007) Trf4 targets ncRNAs from telomeric and rDNA spacer regions and functions in rDNA copy number control. *EMBO J.*, **26**, 4996–5006.
17. Vasiljeva,L., Kim,M., Terzi,N., Soares,L.M. and Buratowski,S. (2008) Transcription termination and RNA degradation contribute to silencing of RNA polymerase II transcription within heterochromatin. *Mol. Cell*, **29**, 313–323.
18. Huertas,P. and Aguilera,A. (2003) Cotranscriptionally formed DNA:RNA hybrids mediate transcription elongation impairment and transcription-associated recombination. *Mol. Cell*, **12**, 711–721.
19. Zhou,R., Zhang,J., Bochman,M.L., Zakian,V.A. and Ha,T. (2014) Periodic DNA patrolling underlies diverse functions of Pif1 on R-loops and G-rich DNA. *eLife*, **3**, e02190.
20. Paeschke,K., Bochman,M.L., Garcia,P.D., Cejka,P., Friedman,K.L., Kowalczykowski,S.C. and Zakian,V.A. (2013) Pif1 family helicases suppress genome instability at G-quadruplex motifs. *Nature*, **497**, 458–462.
21. Omer,C.A. and Faras,A.J. (1982) Mechanism of release of the avian rotavirus tRNATrp primer molecule from viral DNA by ribonuclease H during reverse transcription. *Cell*, **30**, 797–805.
22. Lima,W.F., Murray,H.M., Damle,S.S., Hart,C.E., Hung,G., De Hoyos,C.L., Liang,X.H. and Crooke,S.T. (2016) Viable RNaseH1 knockout mice show RNaseH1 is essential for R loop processing, mitochondrial and liver function. *Nucleic Acids Res.*, **44**, 5299–5312.
23. Mekhail,K., Seebacher,J., Gygi,S.P. and Moazed,D. (2008) Role for perinuclear chromosome tethering in maintenance of genome stability. *Nature*, **456**, 667–670.
24. Smith,J.S., Chen,Q., Yatsunyk,L.A., Nicoludis,J.M., Garcia,M.S., Kranaster,R., Balasubramanian,S., Monchaud,D., Teulade-Fichou,M.P., Abramowitz,L. *et al.* (2011) Rudimentary G-quadruplex-based telomere capping in Saccharomyces cerevisiae. *Nat. Struct. Mol. Biol.*, **18**, 478–485.
25. Salvi,J.S., Chan,J.N., Pettigrew,C., Liu,T.T., Wu,J.D. and Mekhail,K. (2013) Enforcement of a lifespan-sustaining distribution of Sir2 between telomeres, mating-type loci, and rDNA repeats by Rif1. *Aging Cell*, **12**, 67–75.
26. Chan,J.N., Poon,B.P., Salvi,J., Olsen,J.B., Emili,A. and Mekhail,K. (2011) Perinuclear cohibin complexes maintain replicative life span via roles at distinct silent chromatin domains. *Dev. Cell*, **20**, 867–879.
27. Gallo,D., Wang,G., Yip,C.M. and Brown,G.W. (2016) Analysis of replicating yeast chromosomes by DNA combing. *Cold Spring Harb. Protoc.*, **2016**, doi:10.1101/pdb.prot085118.
28. Kobayashi,T. and Ganley,A.R. (2005) Recombination regulation by transcription-induced cohesin dissociation in rDNA repeats. *Science*, **309**, 1581–1584.

29. Saka,K., Ide,S., Ganley,A.R. and Kobayashi,T. (2013) Cellular senescence in yeast is regulated by rDNA noncoding transcription. *Curr. Biol.*, **23**, 1794–1798.
30. Cerritelli,S.M. and Crouch,R.J. (1995) The non-RNase H domain of Saccharomyces cerevisiae RNase H1 binds double-stranded RNA: Magnesium modulates the switch between double-stranded RNA binding and RNase H activity. *RNA*, **1**, 246–259.
31. Gu,Y., Wang,J., Li,S., Kamiya,K., Chen,X. and Zhou,P. (2013) Determination of the biochemical properties of full-length human PIF1 ATPase. *Prion*, **7**, 341–347.
32. Nowotny,M., Gaidamakov,S.A., Crouch,R.J. and Yang,W. (2005) Crystal structures of RNase H bound to an RNA/DNA hybrid: Substrate specificity and metal-dependent catalysis. *Cell*, **121**, 1005–1016.
33. Nowotny,M. and Yang,W. (2006) Stepwise analyses of metal ions in RNase H catalysis from substrate destabilization to product release. *EMBO J.*, **25**, 1924–1933.
34. Kobayashi,T., Heck,D.J., Nomura,M. and Horiuchi,T. (1998) Expansion and contraction of ribosomal DNA repeats in Saccharomyces cerevisiae: Requirement of replication fork blocking (Fob1) protein and the role of RNA polymerase I. *Genes Dev.*, **12**, 3821–3830.
35. Vasiljeva,L., Kim,M., Mutschler,H., Buratowski,S. and Meinhart,A. (2008) The Nrd1-Nab3-Sen1 termination complex interacts with the Ser5-phosphorylated RNA polymerase II C-terminal domain. *Nat. Struct. Mol. Biol.*, **15**, 795–804.
36. Henderson,K.A. and Gottschling,D.E. (2008) A mother's sacrifice: What is she keeping for herself? *Curr. Opin. Cell Biol.*, **20**, 723–728.
37. Santos-Pereira,J.M., Herrero,A.B., Garcia-Rubio,M.L., Marin,A., Moreno,S. and Aguilera,A. (2013) The Npl3 hnRNP prevents R-loop-mediated transcription-replication conflicts and genome instability. *Genes Dev.*, **27**, 2445–2458.
38. Yokoshi,M., Li,Q., Yamamoto,M., Okada,H., Suzuki,Y. and Kawahara,Y. (2014) Direct binding of Ataxin-2 to distinct elements in 3′ UTRs promotes mRNA stability and protein expression. *Mol. Cell*, **55**, 186–198.
39. Elden,A.C., Kim,H.J., Hart,M.P., Chen-Plotkin,A.S., Johnson,B.S., Fang,X., Armakola,M., Geser,F., Greene,R., Lu,M.M. *et al.* (2010) Ataxin-2 intermediate-length polyglutamine expansions are associated with increased risk for ALS. *Nature*, **466**, 1069–1075.
40. Orr,H.T. (2012) Cell biology of spinocerebellar ataxia. *J. Cell Biol.*, **197**, 167–177.
41. Hermosura,M.C., Nayakanti,H., Dorovkov,M.V., Calderon,F.R., Ryazanov,A.G., Haymer,D.S. and Garruto,R.M. (2005) A TRPM7 variant shows altered sensitivity to magnesium that may contribute to the pathogenesis of two Guamanian neurodegenerative disorders. *Proc. Natl. Acad. Sci. U.S.A.*, **102**, 11510–11515.
42. Bhatia,V., Barroso,S.I., Garcia-Rubio,M.L., Tumini,E., Herrera-Moyano,E. and Aguilera,A. (2014) BRCA2 prevents R-loop accumulation and associates with TREX-2 mRNA export factor PCID2. *Nature*, **511**, 362–365.
43. de Baaij,J.H., Hoenderop,J.G. and Bindels,R.J. (2015) Magnesium in man: implications for health and disease. *Physiol. Rev.*, **95**, 1–46.
44. Feeney,K.A., Hansen,L.L., Putker,M., Olivares-Yanez,C., Day,J., Eades,L.J., Larrondo,L.F., Hoyle,N.P., O'Neill,J.S. and van Ooijen,G. (2016) Daily magnesium fluxes regulate cellular timekeeping and energy balance. *Nature*, **532**, 375–379.
45. Haeusler,A.R., Donnelly,C.J., Periz,G., Simko,E.A., Shaw,P.G., Kim,M.S., Maragakis,N.J., Troncoso,J.C., Pandey,A., Sattler,R. *et al.* (2014) C9orf72 nucleotide repeat structures initiate molecular cascades of disease. *Nature*, **507**, 195–200.
46. Skourti-Stathaki,K., Proudfoot,N.J. and Gromak,N. (2011) Human senataxin resolves RNA/DNA hybrids formed at transcriptional pause sites to promote Xrn2-dependent termination. *Mol. Cell*, **42**, 794–805.
47. Szafranski,K., Abraham,K.J. and Mekhail,K. (2015) Non-coding RNA in neural function, disease, and aging. *Front. Genet.*, **6**, 87.
48. Rice,G., Patrick,T., Parmar,R., Taylor,C.F., Aeby,A., Aicardi,J., Artuch,R., Montalto,S.A., Bacino,C.A., Barroso,B. *et al.* (2007) Clinical and molecular phenotype of Aicardi-Goutieres syndrome. *Am. J. Hum. Genet.*, **81**, 713–725.
49. Alzu,A., Bermejo,R., Begnis,M., Lucca,C., Piccini,D., Carotenuto,W., Saponaro,M., Brambati,A., Cocito,A., Foiani,M. *et al.* (2012) Senataxin associates with replication forks to protect fork integrity across RNA-polymerase-II-transcribed genes. *Cell*, **151**, 835–846.
50. Mischo,H.E., Gomez-Gonzalez,B., Grzechnik,P., Rondon,A.G., Wei,W., Steinmetz,L., Aguilera,A. and Proudfoot,N.J. (2011) Yeast Sen1 helicase protects the genome from transcription-associated instability. *Mol. Cell*, **41**, 21–32.
51. Moreira,M.C., Klur,S., Watanabe,M., Nemeth,A.H., Le Ber,I., Moniz,J.C., Tranchant,C., Aubourg,P., Tazir,M., Schols,L. *et al.* (2004) Senataxin, the ortholog of a yeast RNA helicase, is mutant in ataxia-ocular apraxia 2. *Nat. Genet.*, **36**, 225–227.
52. Pulst,S.M., Nechiporuk,A., Nechiporuk,T., Gispert,S., Chen,X.N., Lopes-Cendes,I., Pearlman,S., Starkman,S., Orozco-Diaz,G., Lunkes,A. *et al.* (1996) Moderate expansion of a normally biallelic trinucleotide repeat in spinocerebellar ataxia type 2. *Nat. Genet.*, **14**, 269–276.
53. Sanpei,K., Takano,H., Igarashi,S., Sato,T., Oyake,M., Sasaki,H., Wakisaka,A., Tashiro,K., Ishida,Y., Ikeuchi,T. *et al.* (1996) Identification of the spinocerebellar ataxia type 2 gene using a direct identification of repeat expansion and cloning technique, DIRECT. *Nat. Genet.*, **14**, 277–284.